Desalination and Water Treatment
www.deswater.com
doi: 10.1080/19443994.2015.1021846

57 (2016) 8302–8318
April

Taylor & Francis
Taylor & Francis Group

Removal of humic acid from water by adsorption onto dodecyltrimethylammonium bromide-modified zeolite in a fixed bed reactor

Awad F. Elsheikh, Umi Kalthom Ahmad*, Zainab Ramli

Faculty of Science, Department of Chemistry, Universiti Teknologi Malaysia, UTM Johor Bahru, 81310 Johor, Malaysia, Tel. +60 11 2734 3179; email: awad2003@yahoo.com (A.F. Elsheikh), Tel. +607 5534522; Fax: +607 5566162; email: umikalthom@utm.my (U.K. Ahmad), Tel. +607 5534491; email: zainab@kimia.fs.utm.my (Z. Ramli)

Received 2 July 2014; Accepted 13 February 2015

ABSTRACT

Modification of natural zeolite (NZ; mordenite) surface by a surfactant, dodecyltrimethylammonium bromide (DTAB), was characterized and employed for the removal of humic acid (HA) from water using a fixed bed column. The optimum loading of surfactant was later utilized in adsorption studies. X-ray diffraction spectrum (XRD), Fourier-transform infrared spectrometry (FTIR), nitrogen adsorption–desorption isotherms and Brunauer–Emmett–Teller specific surface area, field emission scanning electron microscopy, and thermographic analysis and derivative thermographic analysis (TGA–DTA) were used to study the surface properties of the NZ and surfactant-modified zeolite (SMZ-DTAB). The effects of a variety of experimental conditions, such as the flow rate (Q), initial HA concentration (C_0), and bed depth (Z), were studied. Optimization studies demonstrated that the SMZ bed with DTAB loading of 150% of ECEC (SMZ-DTAB-150%) exhibited enhanced adsorption performance compared to NZ. An insight of the adsorption mechanism of SMZ-DTAB-150% proved that a monolayer formation is the main viable packing that allows maximum removal of HA. HA adsorption on SMZ-DTAB surfaces is largely a result of the hydrophobic interaction and hydrogen bonding. The adsorption data were utilized on two well-established fixed bed adsorption models, namely Thomas and Adam–Bohart. The results fitted well for Thomas model for the description of whole breakthrough curve with correlation coefficient, $R^2 \geq 0.87$ and low error function value less than 13.

Keywords: Adsorption; Humic acid; Surfactant modified zeolite; Fixed-bed column

1. Introduction

Humic acids (HA) are one of the main components of humic substances (HS) which occur by biological decomposition of natural organic matter (NOM) from plants and other organisms [1,2]. The HA is not directly toxic in water but have undesirable effects on the appearance, which changes the color of the waters from yellow to brown, taste of water, and pose hazard in water treatment processes [3]. Since the early 1970s, water quality and treatment issues related to NOM have been reported [4]. These substances in natural water facilitate bacteria reproduction during drinking water distribution, produce harmful disinfection byproducts during chlorination process, reduce the effectiveness of water purification by interfering with various oxidants, and increase the solubility of heavy

*Corresponding author.

1944-3994/1944-3986 © 2015 Balaban Desalination Publications. All rights reserved.

metals due to complexation with metals and adsorbed organic pollutants [4].

Structural wise, HA are a heterogeneous class of moderate molecular weight, yellow-colored biomolecules existing commonly in all soils, sediments, and natural waters. HA are also the most diffusive natural compounds with complicated and varying structures and are usually resistant to microbial degradation. HA may produce disinfection by products, such as trihalomethanes (THMs) in the process of chlorination. It was known that HA have an effect on the fate of microorganic pollutants (e.g. intake, accumulation, movement, degradation, toxicity, etc.). Recent discovery of HA as a probable cause of Kaschin–Beck and other diseases has brought new light to the removal of HA in the water [5,6].

THMs are frequently found in water treatment systems, existing mainly as chloroform ($CHCl_3$), dichlorobromomethane ($CHBrCl_2$), dibromochloromethane ($CHBr_2Cl$), and bromoform ($CHBr_3$). There are many studies on THM as potentially carcinogenic chlorination byproduct that causes health problems such as bladder cancer, spontaneous abortions, and birth defects [7–9]. Therefore, the removal of HA from water is essential and numerous methods have been developed such as chemical coagulation, membrane separation, advanced oxidation, and adsorption. Among these techniques, adsorption is usually regarded as an optimistic technique and has been extensively studied for removal of HS [10].

Natural zeolites (NZs) are crystalline microporous aluminosilicates with very well distinct structures that consist of a framework shaped by tetrahedrons of SiO_4 and AlO_4. They have permanent negative charge in their crystal structures that can be balanced by exchangeable cations such as Ca^{2+}, Mg^{2+}, K^+, and Na^+. Thus, NZs typically can exchange cations but not anions, which make them suitable for surface modification using cationic surfactants. Previously used surfactants, such as hexadecyltrimethylammonium bromide (HDTMA), n-cetylpyridinium (CPD), benzyltetradecyl ammonium (BDTDA), stearyldimethylbenzylammonium (SDBAC) [11], have been utilized for removal of HS. Wide studies on the use of HDTMA-modified zeolite in removing anionic and organic contaminants and the intercalation of HDTMA into zeolite to remove HS have been conducted [10]. However, there are only a few reports on the use of dodecyltrimethylammonium bromide (DTAB) as surfactant of NZ to afford an adsorbent for enhanced removal of HA from water. This study was designed to investigate the fixed bed column performance of SMZ as an adsorbent for the removal of HA from water in a continuous flow system. The optimum loading of DTAB was applied in characterization, adsorption, and kinetic studies.

2. Materials and methods

2.1. Chemicals and material

The NZ used in the experiments was provided in Malaysia via Chan Chun Chan Enterprise Company. Based on reported methods [12,13], the cation exchange capacity (CEC) of NZ was determined to be 108.3 meq 100 g^{-1} and the ECEC is 0.456 meq g^{-1} determined based on the procedure of Childs. HA was purchased from Tokyo Chemical Industry Co., Japan and purified using the following procedure: 0.4 g of HA was added to 2 L of 4 M NaOH solution volumetric flask producing a 200 ppm stock solution with pH 11. The 100 ppm standard solution was then diluted to the desirable concentrations for spectroscopic analysis. The pH of HA solution was 7.00 ± 0.10 which was adjusted to a given value by adding either 0.1 M HCl or 0.1 M NaOH.

2.2. Preparation of SMZ-DTAB

NZ of 10 g was mixed with varying amounts of DTAB aqueous solutions with 200 mL distilled water in a 400 mL flask. The mixture was then shaken at 150 rpm for 8 h. Surfactant-loading levels ranged from 0 to 200% of ECEC of zeolite (SMZ-DTAB-0% to SMZ-DTAB-200%). The samples were then filtered, washed with distilled water, and dried at 70˚C in an oven for 12 h. Subsequently, the dried SMZ-DTAB was then crushed by passing it through standard ASTM sieves, yielding samples with particle size distribution of ≤0.425 mm [14].

2.3. Characterization

NZ and SMZ-DTAB were subjected to several instrumental characterizations. The X-ray diffraction spectra (XRD) were recorded with a CuKα radiation (λ = 1.5418) at 30 kV and 20 mA ranging from $2\theta = 5^\circ$ to 80˚ and scanning speed of 0.05˚ per second using a Siemens D5000 X-ray Diffractometer (Karlsruhe, Germany). Fourier-transform infrared spectra (FTIR) of NZ and SMZ were recorded between 400 and 4,000 cm^{-1} using a Perkin-Elmer Spectrum TM 400 model FTIR spectrometer (Waltham, MA USA). The Brunauer–Emmett–Teller (BET) method, Barret–Joyner–Halenda (BJH) method, and the single point surface area were used to determine the surface area and the pore diameter distribution of NZ and SMZ using a Micromeritics Model 3Flex Surface Characterization

Analyzer (Atlanta, USA). The samples were degassed by heating up the samples under continuous N_2 purging. The samples were heated up to 90°C for 1 h followed by 350°C for 48 h. N_2 adsorptions were measured at different target pressures under the liquid nitrogen bath, and isotherms were obtained for adsorption/desorption. The surface morphologies of NZ and SMZ-DTAB were examined by field emission scanning electron microscopy (FESEM) and EDX experiments using a Carl Zeiss Model Supra 35-VP FESEM (Oberkochen, Germany). Thermogravimetric analysis (TGA) and derivative thermogravimetric analysis (DTA) of NZ and SMZ-DTAB samples were conducted using a Pyris Diamond Perkin-Elmer (Yokohamo-shi, Japan). The samples were heated from 50 to 1,000°C at a heating rate of 10°C min^{-1} under a N_2 flow rate of 100 mL min^{-1}.

2.4. Adsorption studies

Schematic of experimental fixed bed reactor is shown in Fig. 1. A cylindrical glass column (80 cm in length and 3 cm in diameter) was used with an upward flow of influent. In order to study the effect of flow rate (Q) on the performance of the adsorbent column, flow rates of 12, 18, and 22 mL min^{-1} with linear velocities (F) of 4, 4.5, 5 cm min^{-1}, constant HA concentration of 50 mg L^{-1}, and constant bed depth of 40 cm were applied. The effect of bed depth (Z) on the performance of the adsorbent column was studied using heights 10, 15, and 25 cm (equivalent to 25, 40, and 55 g) with constant HA concentration 50 mg L^{-1} and constant flow rate 18 mL min^{-1}, and in order to study the effect of initial concentration (C_0) of HA on performance of the adsorbent column, concentrations 30, 50, and 70 mg L^{-1} with constant bed depth 15 cm and constant flow rate 18 mL min^{-1} were used. Effluent samples from the column were collected at specified time intervals, and remaining HA concentrations in the solution were measured by a UV/vis spectrophotometer at a wavelength of 254 nm. In all experiments, the temperature value was controlled to 25 ± 0.5°C. The pH of HA solution was 7.00 ± 0.10 adjusted to a given value by adding either 0.1 M HCl or 0.1 M NaOH to study the effect of pH of HA solution.

2.5. Mathematical column models

The loading performance of SMZ-DTAB to adsorb HA from water in a fixed bed reactor was expressed in terms of C_t/C_0 as a function of time of the effluent for a given bed depth, thus the breakthrough curves (BTC) were obtained [15–18]. The maximum column capacity, q_{total} (mg), for a given feed concentration and flow rate (Q, mL min^{-1}) is equal to the area under the plot of the adsorbed HA concentration (C_{ad}, mg L^{-1}) versus effluent time (t, min) and is calculated from Eqs. (1)–(3):

$$q_{total} = \frac{Q}{1,000}\int_{t=0}^{t=t_{total}} C_{ad}\,dt \quad (1)$$

$$C_{ad} = C_0 - C_t \quad (2)$$

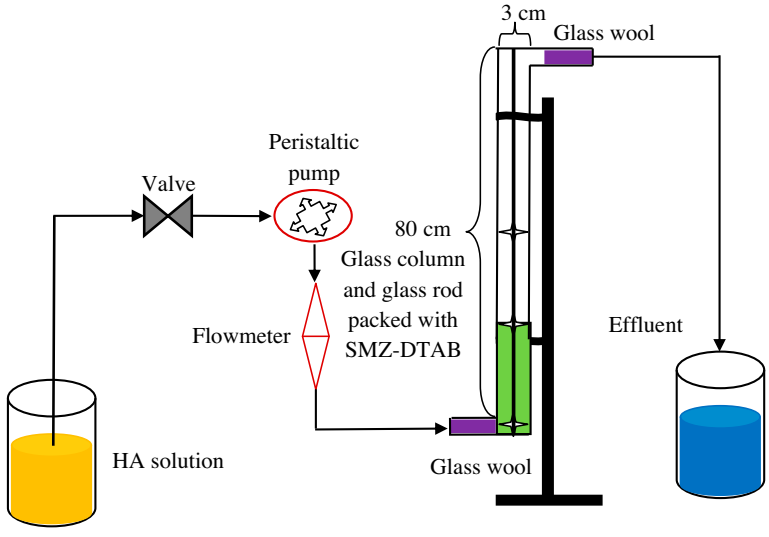

Fig. 1. The schematic diagram of fixed-bed reactor.

$$q_{\text{total}} = \frac{Q}{1,000}\int_{t=0}^{t=t_{\text{total}}} (C_0 - C_t)\mathrm{d}t \quad (3)$$

where Q is volumetric flow rate (mL min^{-1}), C_0 is influent HA concentration (mg L^{-1}), C_t is effluent HA concentration (mg L^{-1}), t is effluent time (min), and t_{total} is total flow time (min). The equilibrium uptake is the weight of HA adsorbed per g of adsorbent from experiment ($q_{e(\text{exp})}$, mg g^{-1}) is calculated from the following Eq. (4) [15–18]:

$$q_{e(\text{exp})} = \frac{q_{\text{total}}}{X} \quad (4)$$

where X is total dry weight of adsorbent in column (g). The total amount of HA delivered to column (M_{total}, mg) is given as in Eq. (5) [15–18]:

$$M_{\text{total}} = \frac{C_0 Q\ t_{\text{total}}}{1,000} \quad (5)$$

The total HA removal efficiency (Y, %) is the relation between the maximum capacity of the column to the total amount of HA sent to column as in Eq. (6) [15–18]:

$$\Upsilon = \frac{q_{\text{total}}}{M_{\text{total}}} \times 100 \quad (6)$$

For the effective design of a column adsorption process, it is significant to predict the BTC for the effluent. Different kinetics models have been developed to predict the dynamic performance of the fixed bed column.

2.5.1. Thomas model

The Thomas model is often used to estimate the maximum adsorption capacity and adsorbent and predict the BTC. The expression of Thomas model for an adsorption column is given in a linearized form in Eq. (7) as follows [15–19]:

$$\ln\left(\frac{C_0}{C_t} - 1\right) = \frac{K_{\text{Th}} q_e \chi}{Q} - K_{\text{Th}} C_0 t \quad (7)$$

where K_{Th} is the rate constant of Thomas model, (mL min^{-1} mg^{-1}), q_e is the equilibrium HA uptake per g of the adsorbent (mg g^{-1}), and t is effluent time, (min). The values of K_{Th} and q_e can be determined from a plot of ln $(C_0/C_t - 1)$ against t using linear regression analysis.

2.5.2. Adams–Bohart model

The Adams–Bohart model is applied for the explanation of the initial part of the BTC. As shown in Eq. (8), the linearized form is as follows [15–19].

$$\ln\left(\frac{C_t}{C_0}\right) = K_{AB} C_0 t - K_{AB} N_0 \frac{Z}{F} \quad (8)$$

where K_{AB} is kinetic constant of Adams–Bohart model (L min^{-1} mg^{-1}), N_0 is maximum adsorption capacity of the adsorbents in terms of saturation concentration from Adams–Bohart model (mg L^{-1}), Z is bed depth of column (cm), and F is linear velocity (cm min^{-1}). From this equation, values describing the characteristic operational parameters of the fixed bed column can be calculated from a plot of $\ln(C_t/C_0)$ against t using linear regression analysis.

2.5.3. Error analysis

The error analysis is used to confirm which model was suitable by applying an error function (SS) as shown in Eq. (9) [18]:

$$\text{SS} = \sqrt{\sum \frac{(y_e - y_c)^2}{n}} \quad (9)$$

where $y_e$is the experimental data, y_c is the predicted (calculated) data, and n is the number of experimental data points. In order to select the best appropriate isotherm for the adsorption system, it is essential to analyze the data using SS, combined with the values of the obtained correlation coefficient (R^2).

3. Results and discussion

3.1. Determination of optimum loading of SMZ-DTAB

The removal of HA by NZ and SMZ-DTAB samples at 0–200% surfactant loading (DTAB) were studied using initial HA concentration (C_t) of 50 mg L^{-1} as in Table 1. The results indicated that all surfactant-modified zeolites (SMZ-DTAB) showed great enhanced adsorption capacity of HA compared to NZ. The concentration of HA adsorbed onto SMZ is

Table 1
Comparison of adsorption capacities of HA and Zeta potential of samples analyzed

Sample	C_{ad} (mg L^{-1})	q_{total} (mg)	$q_{e(exp)}$ (mg g^{-1})	ϒ (%)	Zeta-potential (mV)
NZ-DTAB-0%	38.45	69.21	1.73	76.90	−46.5
SMZ-DTAB-50%	45.75	82.35	2.14	91.50	−31.7
SMZ-DTAB-75%	45.40	81.72	2.05	90.80	−23.4
SMZ-DTAB-100%	46.25	83.25	2.09	92.50	−17.6
SMZ-DTAB-125%	47.65	85.77	2.15	95.30	−9.2
SMZ-DTAB-150%	48.06	86.51	2.16	96.12	0.32
SMZ-DTAB-200%	46.90	84.42	2.11	93.38	13.1

directly related to the percentage loading of DTAB adsorbed on zeolite. The optimum loading of SMZ by DTAB occurred at 150% ECEC which have been used previously in characterization and was used later in kinetic and modeling studies of SMZ-DTAB-150%.

The SMZ-DTAB-150% exhibited the highest uptake ($q_{e(exp)}$) of HA than other loading samples. This may be attributed to two reasons. The higher amount of DTAB adsorbed on NZ leads to the formation of a monolayer of DTAB which covered the zeolite surface, thus, allowing an increase in the adsorption capacity of zeolite. Furthermore, DTAB molecules have a carboxyl group (tail) which facilitates the uptake of HA. Hence, the adsorption of HA on zeolite is dependent upon the presence and the nature of surfactant molecules on the zeolite surface [20–23]. Table 1 also shows that the Zeta potential (ZC-3000) increases with increasing loading of DTAB. The zero point of charge (zpc) was achieved for SMZ-DTAB at 150% ECEC [14]. Above the DTAB loading level of 150% of ECEC, effective volume was reduced leading to a lower adsorption due to the large molecules of HA [24].

This adsorption pattern may reveal why the greatest performance occurred when the DTAB loading was equal to 150% of the ECEC. Based on Table 1, the removal efficiency (γ, %) and adsorption capacity ($q_{e(exp)}$, mg g^{-1}) of SMZ-DTAB are highest for SMZ-DTAB-150% i.e. almost 96.12% and 2.16 mg g^{-1}, respectively, higher than that of NZ (76.90% and 1.73 mg g^{-1}). It was also found that the adsorption capacity is approximately 20% higher than that of NZ.

3.2. Characterization of NZ and SMZ-DTAB

3.2.1. Structural characterization by XRD technique

The X-ray diffractograms of NZ and SMZ at different loadings of DTAB are presented in Fig. 2. The mineralogical composition of NZ was found to comprise primarily of mordenite and additionally of quartz, montmorillonite, and feldspar by means of

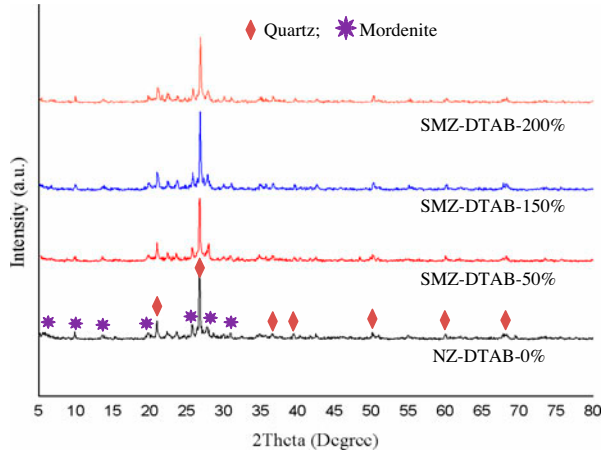

Fig. 2. XRD patterns of NZ and SMZ.

XRD [15,25]. Quartz was detected as a major component in the NZ with 78.13%, while mordenite gave only 21.86% based on the percentage of intensity peaks at I_{100} (intensity at 100) for mordenite and I_{100} for quartz (Fig. 2). The XRD pattern of the SMZ-DTAB is very close to that of the corresponding parent NZ, which indicates that the crystalline nature of the zeolite is kept intact after modification by DTAB molecules (Table 2). The relative intensity (I_{rel}) of X-ray peaks corresponding to some typical crystallographic planes of the NZ and SMZ at different loadings of DTAB are also shown in Table 2. The increased values of I_{rel} for SMZ are as a result of cation-exchange reaction which takes place in NZs when modified by DTAB.

3.2.2. FTIR spectroscopy

Fig. 3 shows the FTIR spectra of NZ, DTAB, and SMZ. The FTIR spectrum of NZ composed of the peaks of sorbed water and the vibrations of zeolite framework T–O (T= Si or Al). The positions of the five

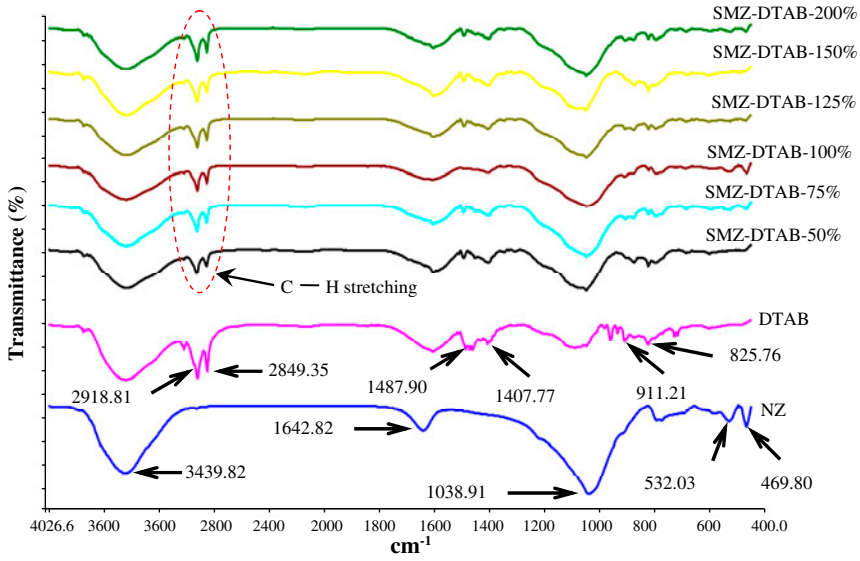

Fig. 3. FTIR spectrum of NZ, DTAB, and SMZ.

main adsorption bands for the NZ were registered at: 3,439, 1,642, 1,038, 532, and 469 cm^{-1}. The vibrations at the 3,439 and 1,642 cm^{-1} are assigned to the presence of hydroxyl group of zeolitic water [15,26]. The band at 1,038 cm^{-1} is attributed to a strong T–O stretching vibration. Band at 532 cm^{-1} is assigned for double six rings for Si–O–T bonds of zeolite framework, while band at 469 cm^{-1} is assigned for bending mode of T–O [27]. The main adsorption bands for the DTAB were assigned as follows: 2,918 and 2,849 (–CH stretching vibration), 1,487 and 1,407 (–CH scissoring vibration), 911 and 825 cm^{-1} (C–O skeletal vibration). The presence of additional peaks at 2,918 and 2,841 cm^{-1} are due to C–H stretching of hydrocarbon originating from the DTAB which is present on the SMZ structure. The frequencies and widths of the CH_2 stretching modes depend highly on the conformation and the packing density of CH_2 chains. Broadening of bands in SMZ-containing DTAB molecules implied a disordered zeolite structure compared to the NZ [20].

3.2.3. Surface area and pore analysis

The adsorption characteristics of zeolites are the products of increased adsorption potential inside the small cavities, and this consists of van der Waals and electrostatic forces. The adsorption potential in addition to the pore structure is the most significant features controlling the adsorption characteristics of zeolite [28]. The pore sizes, especially small ones, were major factors in obtaining high removal efficiency of HA [29–30]. Table 3 shows the surface area and porosity for NZ and loading of higher adsorption capacity, SMZ-DTAB-150%.

Surface area measurements were obtained using three methods, Single point surface area at $P/Po = 0.30$, BET and Langmuir, and porosity details all of which proved that NZ is significantly different from SMZ-DTAB-150%. In order to obtain surface area and porosity details of NZ and SMZ-DTAB-150%, the N_2 adsorption–desorption isotherms and the BJH pore diameter distributions studies were first acquired. The N_2 adsorption–desorption isotherm plots and BJH pore diameter distributions of NZ and SMZ-DTAB-150% are presented in Figs. 4 and 5. The NZ and SMZ-DTAB-150% showed a type IV N_2 adsorption isotherm shape with an obvious hysteresis loop, signifying the presence of mesopores in all samples [26,31]. Furthermore, it can be seen that the hysteresis loop shifts approach relative pressure $(P/P_0) = 1$, to denote the presence of macropores in NZ and SMZ-DTAB-150%. Otherwise, the adsorption process on mesoporous solids is often accompanied via adsorption–desorption hysteresis [31]. Therefore, the isotherms demonstrated a type H4 loops characteristic for parallel and roughly horizontal branches and their appearance has been attributed to adsorption–desorption in thin slit-like pores. The Type H4 loop indicated that the zeolite particles have internal voids of uneven shape and wide size distribution. The hysteresis of type H4 also exhibited hollow spheres with walls composed of ordered mesoporous silica. This would propose that H4 hysteresis loops may only occur from the existence of large

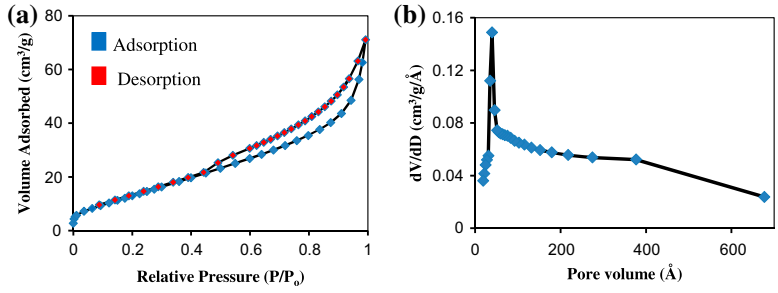

Fig. 4. N_2 adsorption–desorption isotherms (a) and BJH pore diameter distributions (b) of NZ.

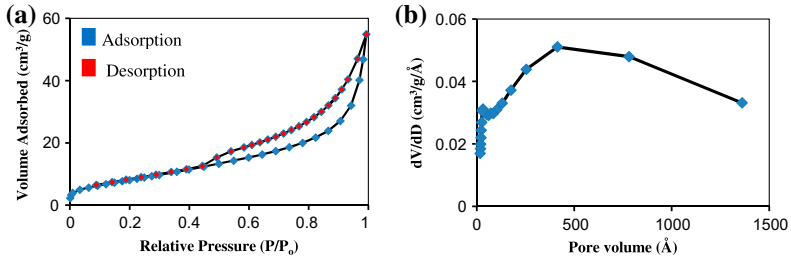

Fig. 5. N_2 adsorption–desorption isotherms (a) and BJH pore diameter distributions (b) of SMZ-DTAB-150%.

mesopores entrenched in a matrix with pores of many smaller sizes. In contrast, The isotherm for NZ and SMZ-DTAB-150% showed an obvious and light wide hysteresis loop at relative pressure of 0.45, which is distinctive for mesoporous zeolite of ink bottle-type pores with pore necks lesser than 4 nm (Figs. 4(a) and 5(a)). NZ and SMZ-DTAB-150% had a high ratio of mesoporous volume, which was in good conformity with the results in Table 3 [32]. These analyses agreed well with BJH pore diameter distributions of NZ and SMPZs (Figs. 4(b) and 5(b)), which confirmed that the NZ and SMZ-DTAB-150% have a wide pore diameter distribution in mesoporous domains. Bigger pore size makes wider surface area of the materials thereby giving more exchange sites and resulted in higher adsorption capacity [33]. Pure zeolites contain almost micropores and external surface area, but after subjected to different treatment, a mesoporous structure could be created [34].

The high surface area for NZ can provide more sites for cationic surfactants to be adsorbed onto NZ. The surface area of NZ becomes smaller after modified using DTAB as a result of a layer of surfactant surrounded zeolite particles resulting in the larger pore size. Also, the surface area measurement for adsorption capacity is important for the HA removal efficiency. In general, a larger surface area translates into a greater adsorption capacity. The pore volumes of NZ also decreased when it was modified with the cationic surfactants DTAB (Table 3). The pore size data using BET and BJH revealed that the SMZ-DTAB-150% are higher than NZ. A probable explanation is that the cationic surfactant blocked in a greater proportion the smallest pore diameters and so, the average pore diameter increased [35]. This implies that adsorption in this zeolite is not a surface process, but is rather a volume filling.

On the other hand, the results of the density functional theory (DFT) (Table 3) establish the presence of additional porosity at <10.22 Å after modification and did not exist in the NZ, which arises as a result of the interstitial voids existing between the nanopores [36]. This also explains the reason for the high absorption capacity of SMZ-DTAB-150%. Table 3 indicates using Horvath–Kawazoe pore size that the maximum pore volume and median pore width of NZ decreased after modification [37]. The result is in good agreement with the average results from DFT pore size.

An important aspect in the characterization of microporous solids is the evaluation of the parameters that characterize the microporous structure. Dubinin–Radushkevich (DR), and Dubinin–Astakhov (DA) have equations for describing the physical adsorption of gases on microporous solids [38–40]. The results of DR and DA reflected the role of surfactants to reduce the micropore surface area of NZ which in turn affects the adsorption capacity of SMZ (Table 3). Moreover, the DR and DA data show monolayer capacity and

limiting micropore volume of NZ have decreased after modification by cationic surfactant. It indicates that the nanoporosity and mesoporosity of NZ gradually decreases due to the cationic surfactant modified [41].

Overall, based on all results of surface area and porosity details, it was found that the surface area and pore volume decreased after modification, while pore size increased by DTAB. This is part of the main reasons that enabled the SMZ-DTAB-150% to have enhanced adsorption capacity for HA compared to NZ.

3.2.4. Surface morphological and elemental analysis

The morphological characteristics of NZ (mordenite) and SMZ-DTAB-150% were captured using FE-SEM. The results are presented in Fig. 6 with a resolution of 1 μm to show the modification of zeolite by DTAB. Fig. 6(a) exhibited a distinct flowery pattern with some sheet-like morphology for NZ. Conversely, the SMZ-DTAB-150% represents an image of an uneven surface (Fig. 6(b)). These results indicate that an organic layer was shaped on the surface of NZ after being modified by DTAB. The results of EDX elemental analysis are obtainable in Table 4. Because energy dispersive is less sensitive to elements with atomic numbers less than 20, the weight percents listed in the related tables in these figures has been considered on an oxygen-free basis [42]. The cations of NZ comprise of Na^+, K^+, and Mg^{2+} as well as Fe^{3+} from the heavy metal groups to balance the negative charge of zeolites framework. The elemental composition obtained indicates that the elemental weight percentages of carbon ions raise from near zero in NZ to 15.05% in SMZ-DTAB-150%, which indicates the presence of surfactant that interact with NZ surface. Furthermore, the higher percentage of carbon ions is a significant indicator of its existence with a large amount of alkyl group on zeolite surface and explains the reason for SMZ-DTAB-150%-enhanced ability to remove HA compared to other samples.

The elemental weight percentages of magnesium, potassium, and iron ions resulted from SMZ were found to vary. The ion exchange occurred for K^+, Mg^{++}, and Fe^{++} rather than Na^+ due to zeolite modification which in turn affects the surface area, thus pore size to allow ion exchange. The percentage of Na^+ in EDX spectrum of sample NZ is near to zero. After zeolite modification, the sodium ion percentage increased with increasing adsorption capacity. Sodium ions included within the interparallel pore are more difficult to recover via ion exchange [43]. The larger pore size of SMZ, as noted previously, provides a more facile passage for metal ions and increases its resulting exchange rate compared to NZ.

The chemical and physical properties of the zeolite depend substantially on the silica to alumina ratio (SAR) in the framework [44]. The model unit cell formula of mordenite is known as Na_8 $[(Al_2O_3)_4$ $(SiO_2)_{40}].24H_2O$. This demonstrates a silica/alumina ratio of 10:1 [45]. The presence of the negative framework and the positive cations encourage strong electrostatic field on the zeolite surface, this affects the interaction capacities with polar molecules such as water. SAR of NZ and SMZ-DTAB-150% define the chemical composition of the zeolite framework structure, where zeolite with low SAR will include high amount of Al in the zeolite framework. In this study, as indicated in Table 4, the present NZ (mordenite) has a lower SAR (3.47%) compared with other types of zeolites previously used [44–46], hence leading to higher load (amount) of surfactant attached to zeolite surface. The results also showed that the Si element of SMZ-DTAB-150% deceased significantly with

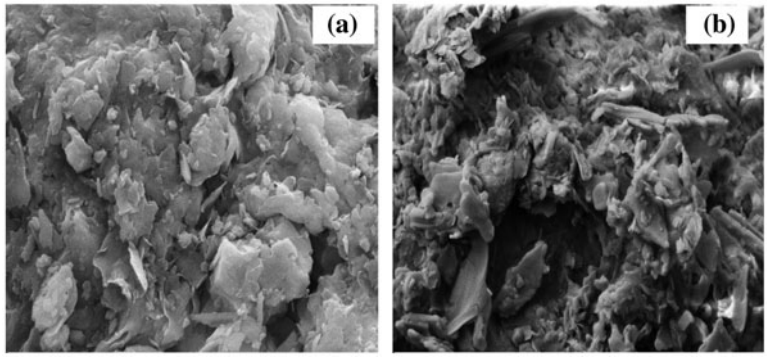

Fig. 6. SEM micrographs of (a) NZ and (b) SMPZ-DTAB-150% at 10.00 K X modification.

increasing amount of surfactants. In contrast, percentage of Al element has not changed considerably. This is due to the presence of aluminum in center of framework of zeolite that is less affected by additional surfactant, while silicon, inside of framework, is more affected by cationic surfactants [47,48]. On the other hand, the deceased of SAR for different SMZ-DTAB-150% has lead to increasing adsorption of HA from water. Thus, the modification of NZ by DTAB decreased SAR as result of the change in electronegativity by reducing Si element and pore size distribution of the zeolite. Therefore, the SAR has effected the surface properties and their framework flexibility [49].

3.2.5. Thermal analysis

Thermogravimetric analysis (TGA) is also performed as an important thermal analysis for the study of hydrated state in porous zeolite and displays the thermal stability of the materials [26]. The TGA curve for NZ is shown in Fig. S1. There were two stages of weight loss observed. The maximum weight loss for external water was released up to 285˚C followed by a slowed weight loss up to about 980˚C. After 285˚C, the NZ started to lose its loosely and tightly bound water [26,50]. The total weight loss up to 980˚C was calculated as 6.77 %. This value was reported as 7 % in both studies of Arletti et al. [51] and also Martucci et al. [52]. The loss shown in the DTG curve is as a result of water molecules weakly bound to the zeolite surface for loss below 100˚C, and water molecules inside the channel, contributing to loss at higher temperatures. Based on the result of DTG analyses, the amount of water on the surface of the mordenite zeolite corresponds to about 2.50% in weight, whereas the structural water or hydroxide group accounting for the residual weight loss represents about 4%. The main intensive derivative curve peaks due to loss of water molecules were observed from DTA at below 80˚C.

In contrast, the TGA curves for SMZs revealed three stages of weight loss (Fig. S2). At low temperature, the DTG curve of the SMZ-DTAB-150% and NZ shows a similar behavior (with a loss around 3% at 100˚C). The weight loss between 30 and 200˚C for SMPZ-DTAB-150 % is 2.06. This result suggested that the DTAB have a great ability to replace external water molecules due to their small size. This has been previously observed in the literature [53] which was also proved by porosity analysis (Table 3) where the SMZ-DTAB-150% was shown to have a higher pore size. Moreover, results of TGA show NZ are hydrophilic materials where the total weight lost due to water molecules loss are higher (6.77%) compared to SMZ-DTAB-150% (5.66%). This was due to the formation of the monolayer of cationic surfactant that changed into hydrophobic layer [53].

The weight loss above 200˚C, which corresponds to 8.59 mg, can be ascribed to desorption and/or decomposition of DTAB from zeolite pores at about 600˚C. DTAB existed as residual surfactants on the NZ structure at 600˚C. Based on previous studies [54–56], the decomposition of cationic surfactant within SMZ usually take places in two phases; the first phase corresponds to the decomposition of surfactants connected to their adjacent molecules during hydrophobic interaction and the second phase results from the removal of surfactants connected to the surface of zeolite during electrostatic interaction. The occurrence of the derivative curve peak (DTA) appeared between 200 and 300˚C in the SMZ-DTAB-150% DTA curve. This indicated the presence of DTAB on external zeolite surface [50,51]. Similar curve was absent in the NZ DTA curve and confirmed that some cationic surfactants' molecules had been bound to the zeolite surface via electrostatic interaction after the modification process [26].

3.2.6. Proposed adsorption mechanisms of HA by SMZ and effect of surfactants loading levels of DTAB

The removal of HA by SMZ-DTAB occurs by two major mechanisms, the chemical and physical adsorption. The chemical adsorption mechanisms have been proposed as follows: hydrophobic interaction, hydrogen bonding, van der Waals interactions, and electrostatic attraction [54,57]. The binding between cationic surfactant DTAB and HA is caused by electrostatic and hydrophobic attractions. This indicates that hydrophobic interaction or electrostatic attraction may play a significant role in HA adsorption onto DTAB modified zeolite [14,24]. Also, the configuration of hydrogen bonds between C or N of DTAB and hydroxyl groups and carboxylic groups of HA may be suitable to HA adsorption onto SMZ-DTAB.

The Zeta potential that varied with different DTAB loadings (Table 1) reflects the change between monolayer and bilayer coverage on the SMZ-DTAB. Proposed surfactant formations of adsorbed surfactant molecules are illustrated in Fig. S3. The zeolite surface increasingly loses its negative charge with increasing DTAB loading and changed from hydrophilic to hydrophobic [14].

The physical adsorption of HA by SMZ-DTAB including several phases, at the 0% loading of DTAB, is relatively insignificant perhaps because of the strong dipole interaction between NZ and

water, which prevents the HA adsorption on zeolite surface [23,26].

The mechanism of HA removal from water have varied after NZ was modified by DTAB. Fig. S3 (Supplementary data) explains through the stages of proposed schematic diagram of cationic surfactant molecules (DTAB) on the negative surface of NZ. The resultant hydrophobic organic monolayer surface would encourage more contact and interaction with soluble HA, in order improving the adsorption of HA by van der Waals interactions (Fig. S3(a)). The high number of hydrogen bonds between C or N of DTAB and hydroxyl groups, carboxylic groups, and phenolic groups of HA guarantees additional effective adsorption of HA. At the same time, the zpc at submonolayer sorption of SMZ-DTAB-50% until 125%, the distribution, and hence the density of DTAB in the NZ are controlled by the charge on the zeolite surface. Because the DTAB is a high molecular weight surfactant, (308.34 g mol^{-1}) it cannot penetrate the internal micropores of NZ channels and therefore are only able to access the external surface area. The NZ contain simply micropores and external surface area, but after modification with DTAB, a mesoporous structure could be formed [14,20]. Also at submonolayer, the DTAB forms hemimicelle at the solid–aqueous interface via a cationic exchange process at surfactant concentration at or below its critical micelle concentration (CMC) [58].

At SMZ-DTAB-150%, utmost hydrophobicity encourages higher contact and interaction; hence, SMZ favors a large amount adsorption of HA at this point. Hydrogen bonds also exist among the functional groups of HA. The amount of interparallel pores size at this point is at the maximum making it possible for a higher adsorption rate of HA molecules (Table 3 and Fig. S3(b)). The zpc, at SMZ-DTAB-150%, may correspond to a complete monolayer surface coverage by DTAB, which means it is a best pointer for a surface showing utmost hydrophobicity. Optimal amount of DTAB takes place at loading level 150% of ECEC where the DTAB is expecting to appear as a monolayer on the external surface of the NZ with the lower surface held by the electrostatic attraction between the negatively charged zeolite surface and the positively charged DTAB head groups (Fig. S3(b)).

Furthermore, the characterizations of NZ and SMZ-DTAB explained the principal reasons that affected the adsorption of HA. The loading of DTAB will lead to deceased surface area and porosity of zeolite samples (Table 3). XRD results (Table 2) show reduced relative intensity also the silica alumina ratio (Table 4) which in turn cause low adsorption capacity of HA (Fig. S3(c) and (d)). Moreover, the conformation (or the gauche/trans conformed ratio) and the packing density of methylene chains determined the frequencies and widths of the CH_2 stretching modes [24]. For the all-trans alkyl chain of crystalline DTAB, FTIR spectra (Fig. 3) showed the positions of CH_2 asymmetric and symmetric stretching modes are around 2,918 and 2,849 cm^{-1}, respectively. If conformations disorder is involved in the chains, their positions would change to higher wavenumber, depending upon the average content of gauche conformers [24]. Meaningful differences in frequencies between the SMZ-DTAB and the crystalline DTAB indicated that DTAB molecules on the SMZ have a more disordered structure than the crystalline DTAB.

Fig. S3(c) and (d) illustrates that above SMZ-DTAB-150%, an effective compact volume also causes a lower adsorption. This adsorption behavior may disclose why the higher adsorption capacity occurred at the loading DTAB 150% of ECEC without the others [59]. Values above zpc at multilayer of DTAB molecules tend to reduce the surface area and alter surface charge. Thus, interparticle size becomes lesser for the HA to enter and be adsorbed and again, the surface be converted into hydrophilic [59]. Therefore, the aqueous cationic surfactant concentration is larger than the CMC and sufficient amount surfactant exist in solution; the loaded cationic surfactants on the external surface of zeolites form a bilayer, above CMC [24,60]. The upper surface is therefore connected to the lower surface through the hydrophobic interaction between the DTAB and tail groups in both surfaces (Fig. S3(d)).

3.2.7. Influence of operating conditions on column adsorption of HA

3.2.7.1. Effect of feed flow rate on BTC. The effect of flow rate of HA in the form of the BTCs of SMZ-DTAB-150% is shown in Fig. 7. The breakthrough time was found to increase with decreasing flow rate with flow rate 12, 18, and 22 mL min^{-1} gave around 10, 80, and 70 min, respectively. At higher flow rate, BTC occurs at shorter time with the remaining HA still higher in the effluent. The lower feed flow rates induced more effective removal of HA, as can be seen, lower HA remains in the effluent from the lowest flow rate curve. These results could be demonstrated by the retention time of HA ions and mass transfer inside the column packing. At a lower flow rate of adsorbent, HA had more time to be in contact with adsorbent, which lead to a greater adsorption of HA molecules in fixed bed as a result of the higher empty bed contact time [26,61]. Many HA ions would then directly go through the column packing and interact with the

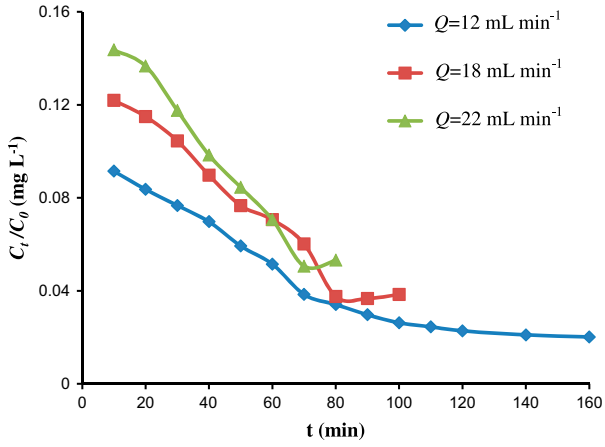

Fig. 7. BTCs: the effect of different feed flow rates (Q) on HA adsorption using SMZ-DTAB-150% at $C_0 = 50$ mg L^{-1}, $Z = 15$ cm and pH 7.00.

adsorbents. As a result, this reduced the effluent HA level, leading to delayed breakthrough and thus, improve the performance of SMZ adsorbent. As a consequence, HA removal increased at the breakthrough point when the inlet flow rate decreased.

3.2.7.2. Effect of column bed depth on BTC. In this study, the SMZ-DTAB-150% were packed in the columns with bed depth (Z) ranging from 10 to 20 cm. The influent HA concentration and the feed flow rate in the fixed bed reactor were fixed at 50 mg L^{-1} and 18 mL min^{-1}, respectively (Fig. 8). The results illustrate that the volume of breakthrough changes with bed depth. As BTC at the bed height (adsorbent mass) increases, the HA had more time to be in contact with SMZ-DTAB-150% that led to higher removal efficiency of HA molecules in column. Thus, the higher bed depth led to a decrease in the HA concentration at the same service time. High removal was observed at the highest bed depth. This was because of an increase in the surface area of adsorbent, which provided more binding sites for uptake. It was also clear that at the greatest bed depth, the contact time also increased as a result of the increased binding sites of the column [26,61].

3.2.7.3. Effect of influent HA concentration on BTC. The fixed bed adsorption was performed by feeding the HA influent with HA concentrations (C_0) of 30, 50, and 70 mg L^{-1}. The inlet upward flow rate of the influent and the bed depth of the column were fixed at 18 mL $min^{-1}$and 15 cm, respectively (Fig. 9). It can be seen that the BTC generally occurred faster with a higher influent HA concentration. Breakthrough time reaching saturation was increased appreciably with an increase in the influent HA concentration. These results indicated that the change in concentration gradient impacts the saturation rate and breakthrough time. This is as a result of an increase in mass driving force which allows more HA to pass from the aqueous solution to the adsorbent surface [16,19,61]. This in turn led to more adsorption sites being covered as the HA concentration increases.

In most operating conditions on column adsorption of HA, the rate of C_t/C_0 decreased gradually with an increase in influent time to reach almost a constant value. However, the result that we obtained is different from the usual trend of the adsorption behavior of SMZ where the C_t/C_0 increases with time. Our result

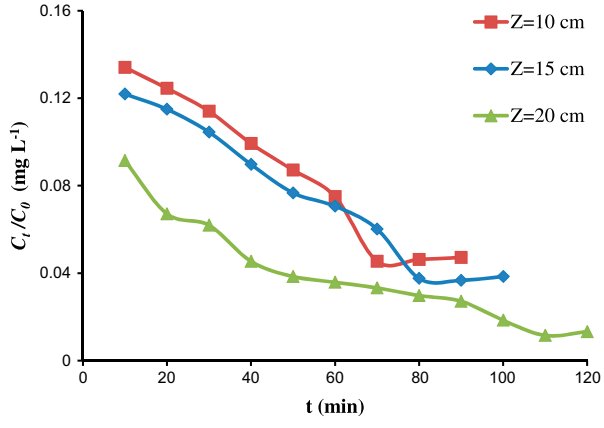

Fig. 8. BTCs: the effect of different bed depths on HA adsorption of SMZ-DTAB-150% at $Q = 18$ mL min^{-1}, $C_0 = 50$ mg L^{-1} and pH 7.00.

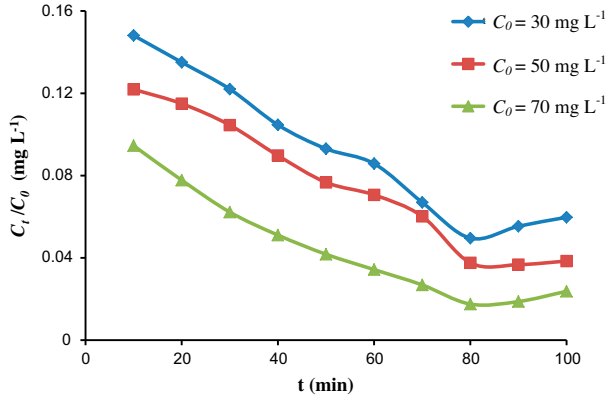

Fig. 9. BTCs: the effect of different influent concentrations on HA adsorption using SMZ-DTAB-150% at $Q = 18$ mL min^{-1}, $Z = 15$ cm and pH 7.

can be explained in terms of the duration of time for the adsorption process took place. In this study, it was observed that most of the adsorption took place within one hour of contact time, while previous studies have more than two hours. Thus, it is expected that the C_t/C_0 increases with increasing contact time of the adsorption process for more than three hours. In that short time of adsorption, the rate of adsorption onto a SMZ-DTAB-150% surface depends upon a number of parameters such as structural properties of the adsorbent, initial concentrations of the HA, and the interaction between the HA and the active sites of the SMZ-DTAB-150%. However, the adsorption process is considered as a surface phenomenon, the possibility of intraparticle diffusion into porous adsorbent can be possible. The pore size distribution plays a more important role than the surface area, in the adsorption process. In any porous materials, particularly in a dynamic system, the major resistance to mass transfer occurs during the movement or diffusion of solute within the pores of the particles [62]. Also, HA adsorption is depended on formed bonding between two hydrophobic surfaces, SMZ-DTAB-150% and HA. Hence, fixed bed adsorption experiments providing for longer times before breakthrough were performed due to low friction loss associated with passing HA through powder surfactant zeolite beds. In addition, that specific or electrostatic interaction become more rapid with increasing contact time, since repulsion is reduced [63].

3.2.8. Evaluation of HA adsorption in fixed-bed column

3.2.8.1. Evaluation of Thomas model. To determine the equilibrium HA uptake (q_e) to the adsorbent and rate constant of Thomas model (K_{Th}), experimental data were fitted into Eq. (7). The simulated breakthrough profiles and the modeling parameters are obtainable in Supplementary data, Figs. S4, S5, and S6, respectively, and Table 5. Linear regression results and values of R^2 are listed in Table 5, where values of R^2 ranged from 0.87 to 0.92 with the SS between 6 and 13. Consistent with Table 2, the calculated q_e from Thomas model is greater than the experimental $q_{e(exp)}$. It is also seen in Table 5 that as flow rate and adsorbent weight increased, the value of q_e decreased, other than the value of k_{Th} increased. As initial concentration increases, the value of q_e and k_{Th} increased and decreased, respectively. Accordingly, the experimental data are in good agreement with the theoretical results (Table 5).

3.2.8.2. Evaluation of Adams–Bohart model. Linear regression results (Table 6) demonstrated that the kinetic constant of Adams–Bohart model (K_{AB}) and maximum adsorption capacity of the adsorbents of the adsorbent (N_0) increased and decreased, respectively, with increasing flow rate and adsorbent weight. This is as a result of additional saturation of adsorbent sites N_0 that decreased with increasing flow rate. On the other hand, both K_{AB} and N_0 deceased with increasing column length. Linear plots of Adams–Bohart model in different heights, flow rates, and concentrations are presented in supplementary data, Figs. S7, S8, and S9, respectively. The predicted curves from the Adams–Bohart model were compared with the corresponding experimental data at different experimental conditions. There is a good agreement between the experimental data and the predicted values. However, the results of linearized simulation were found to have lower

Table 2
Typical X-ray peaks of NZ and SMZ-DTAB

	NZ		SMZ-DTAB-50%		SMZ-DTAB-150%		SMZ-DTAB-200%	
2θ	d (A°)	I_{rel}	d (A°)	I_{rel}	d (A°)	I_{rel}	d (A°)	I_{rel}
9.87	8.95	10.4	8.98	11.9	9.06	12.4	9.07	11.1
13.58	6.51	6.10	6.56	8.30	6.54	8.20	6.58	7.00
19.74	4.49	9.70	4.48	9.10	4.52	9.60	4.52	9.90
22.29	3.98	12.8	3.97	15.7	4.00	15.9	3.99	11.1
25.73	3.45	22.4	3.46	14.1	3.48	14.9	3.47	13.3
26.71	3.33	100	3.33	100	3.35	100	3.35	100
27.70	3.21	18.0	3.21	14.3	3.23	13.8	3.22	15.5
29.98	2.97	7.70	2.98	8.20	2.99	7.50	2.99	8.90
30.92	2.88	10.10	2.89	11.0	2.90	10.4	2.89	6.10

Note: d: interplanar spacing; $I_{rel} = I/I_{max}$: relative intensity.

Table 3
The surface area and porosity details of NZ and SMZ-DTAB-150%

Zeolites	NZ	SMZ-DTAB-150%
Surface area ($m^2 g^{-1}$)		
Single point	49.6406	29.6313
BET	53.3903	29.8824
Langmuir	112.0103	46.2639
Pore volume ($cm^3 g^{-1}$)		
Single point adsorption	0.094865	0.069493
Single point desorption	0.097818	0.072859
Pore size (Å)		
BET adsorption APD	71.0731	93.0224
BET desorption APD	73.2849	97.5273
BJH adsorption APD	74.256	107.127
BJH desorption APD	67.720	86.580
DFT pore size		
Volume in pores < 10.22 Å ($cm^3 g^{-1}$)	0.0000	0.00404
Total volume in pores ≤ 318.00 Å ($cm^3 g^{-1}$)	0.07267	0.04168
Total area in pores ≥ 10.22 Å ($m^2 g^{-1}$)	39.052	26.307
Horvath–Kawazoe		
Maximum PV ($cm^3 g^{-1}$)	0.018759	0.011880
Median pore width (Å)	12.601	11.512
Dubinin–Radushkevich		
Micropore SA ($m^2 g^{-1}$)	42.8679	30.6450
Monolayer capacity ($cm^3 g^{-1}$)	9.848852	7.040664
Dubinin–Astakhov		
Micropore SA ($m^2 g^{-1}$)	43.8830	28.9844
Limiting MV ($cm^3 g^{-1}$)	0.024710	0.016204

Note: APD: Average pore diameter; PV: Pore volume; SA: Surface area; MV: Micropore volume.

correlation coefficient value (R^2 between 0.83 and 0.91) and also greater error function value (SS more than 11) as compared to Thomas model, thus it does not display reliability of the Adams–Bohart model. However, such model is still valid for the relative concentration region up to 0.5.

Table 4
Composition of major elements (%) in NZ and SMZ-DTAB-150% by EDX

Major elements	NZ	SMZ-DTAB-150%
C	0.00	15.05
Na	0.29	0.45
Si	28.45	24.66
Al	8.21	10.54
Mg	1.11	0.14
K	4.58	0.40
Fe	3.30	5.05
Si/Al	3.47	2.34

3.3. Comparison with other different solid adsorbents

Distinct types of natural and synthetic adsorbents were used in HA removal from water. HA adsorption on a variety of adsorbents was widely referred to in the literature. Table 7 gives a comparison on HA uptake capacities of some natural, modified, and synthetic adsorbents, based on mg of HA adsorbed per gram mass of adsorbent. The capacities of the sorbents depend on types of HA and adsorption conditions.

From Table 7, the highest capacity of pillared bentonite is due to the highest BET surface area (111.3 $m^2 g^{-1}$) [65]. The adsorption capacity of SMZ-DTAB-150% is comparable to other adsorbents [67]. The maximum adsorption capacity (q_e) achieved with SMZ-DTAB-150% is 2.16 mg g^{-1}, which is acceptable for SMZ-DTAB-150% to be an adsorbent, with the benefit of easy handling and cost effectiveness. Zeolite modified with DTAB proves as an attractive alternative for HA adsorption.

Table 5
Thomas model parameters using linear regression analysis for HA adsorption to SMZ-DTAB-150% under various operating conditions

Q (mL min^{-1})	Z (cm)	C_0 (mg L^{-1})	K_{Th} (mL min^{-1} mg^{-1})	q_e (mg g^{-1})	R^2	$q_{e\ (exp)}$ (mg g^{-1})	γ (%)	SS
12	15	50	0.246	2.70	0.92	2.35	97.99	12.07
18	15	50	0.324	2.38	0.91	2.17	96.17	9.22
22	15	50	0.356	2.36	0.87	2.08	94.69	6.59
18	10	50	0.336	3.44	0.91	3.09	95.31	8.43
18	20	50	0.322	2.30	0.90	1.94	98.69	12.41
18	15	30	0.454	1.60	0.91	1.27	94.04	8.99
18	15	70	0.280	3.39	0.91	3.08	97.63	10.55

Table 6
Adams–Bohart model parameters using linear regression analysis for HA adsorption to SMZ-DTAB-150% under various operating conditions

Q (mL min^{-1})	Z (cm)	C_0 (mg L^{-1})	K_{AB} (L mg^{-1} min^{-1})	N_0 (mg L^{-1})	R^2	SS
12	15	50	0.24	26.29	0.83	11.70
18	15	50	0.30	18.52	0.90	12.03
22	15	50	0.32	17.49	0.91	11.22
18	10	50	0.31	25.62	0.91	11.68
18	20	50	0.34	17.50	0.89	11.29
18	15	30	0.41	12.96	0.89	12.00
18	15	70	0.26	25.00	0.90	10.97

Table 7
Comparison of adsorption capacity of various adsorbents towards humic acid

Adsorbent	Adsorption capacity (mg g^{-1})	References
SMZ-DTAB-150%	2.16	This study
CPB-modified zeolite	92	[24]
Surfactant-modified chitosan/zeolite composite	164	[26]
Metal-modified silica	1.5–3.6	[64]
	0.2–3.6	
Pillared bentonite	537	[65]
Activated sludge	2.4	[66]
Rice husk ash	2.7	[67]
Modified rice husk ash-NH_2	8.2	[67]

4. Conclusions

In this study, NZ (mordenite) has been successfully modified using DTAB as a surfactant as characterized using XRD, FTIR, surface area and pore size, FESEM, and TGA analysis. Experimental and theoretical investigations carried out to evaluate the fixed bed column performance of HA removal from water onto the surfactant-modified zeolite at 150% ECEC loading of DTAB gave the optimal operating conditions for the fixed bed reactor employed a feed flow rate of 12 mL min^{-1}, adsorbent bed depth of 20 cm, and HA influent concentration of 70 mg L^{-1}. The results showed that SMZ-DTAB was an effective adsorbent for the removal of HA from water. The transient stage

or working stage of the BTC fitted well by the Thomas models using linear regression analysis for HA adsorption under all experimental conditions studied, while the initial region of the BTC was described well by the Adams–Bohart model. It is proposed that the hydrophobic nature of a DTAB monolayer interacts with HA which in turn contributed to the enhanced HA adsorption on SMZ-DTAB surfaces mainly as a result of the hydrophobic interaction, hydrogen bonding, and partitioning mechanism.

Supplementary material

The supplementary material for this paper is available online at http://dx.doi.10.1080/19443994.2015.1021846.

Acknowledgments

Thanks are due to the Ministry of Higher Education Malaysia for financial aid under GUP grant (Q.J130000.7326.02J7) and to the Ministry of Higher Education Libya for scholarship to Awad F. Elsheikh.

References

[1] A. Imyim, E. Prapalimrungsi, Humic acids removal from water by aminopropyl functionalized rice husk ash, J. Hazard. Mater. 184 (2010) 775–781.
[2] M. Wang, L. Liao, X. Zhang, Z. Li, Adsorption of low concentration humic acid from water by palygorskite, Appl. Clay Sci. 67–68 (2012) 164–168.
[3] S. Wang, T. Terdkiatburana, M.O. Tadé, Adsorption of Cu(II), Pb(II) and humic acid on natural zeolite tuff in single and binary systems, Sep. Purif. Technol. 62 (2008) 64–70.
[4] C. Ding, C. Shang, Mechanisms controlling adsorption of natural organic matter on surfactant-modified iron oxide-coated sand, Water Res. 44 (2010) 3651–3658.
[5] J. Yang, J. Jia, J. Liao, Y. Wang, Removal of fulvic acid from water electrochemically using active carbon fiber electrode, Water Res. 38 (2004) 4353–4360.
[6] X. Yang, C. Shang, P. Westerhoff, Factors affecting formation of haloacetonitriles haloketones, chloropicrin and cyanogen halides during chloramination, Water Res. 41 (2007) 1193–1200.
[7] M. Panyakapo, S. Soontornchai, P. Paopuree, Cancer risk assessment from exposure to trihalomethanes in tap water and swimming pool water, J. Environ. Sci. 20 (2008) 372–378.
[8] J. Lee, K.T. Ha, K.D. Zoh, Characteristics of trihalomethane (THM) production and associated health risk assessment in swimming pool waters treated with different disinfection methods, Sci. Total Environ. 407 (2009) 1990–1997.
[9] W. Lee, P. Westerhoff, Formation of organic chloramines during water disinfection–chlorination versus chloramination, Water Res. 43 (2009) 2233–2239.
[10] Y. Zhan, J. Lin, Z. Zhu, Removal of nitrate from aqueous solution using cetylpyridinium bromide (CPB) modified zeolite as adsorbent, J. Hazard. Mater. 186 (2011) 1972–1978.
[11] S. Wang, Y. Peng, Natural zeolites as effective adsorbents in water and wastewater treatment, Chem. Eng. J. 156 (2010) 11–24.
[12] C.W. Childs, Clay Mineralogy: Spectroscopy and Chemical Determinative Methods, Chapman and Hall, London, 1994.
[13] S.J. Kang, K. Egashira, Modification of different grades of Korean natural zeolites for increasing cation exchange capacity, Appl. Clay Sci. 12 (1997) 131–144.
[14] S.G. Wang, W.X. Gong, X.W. Liu, B.Y. Gao, Q.Y. Yue, D.H. Zhang, Removal of fulvic acids from aqueous solutions via surfactant modified zeolite, Chem. Res. Chin. Univ. 22 (2006) 566–570.
[15] R. Han, Y. Wang, X. Zhao, Y. Wang, F. Xie, J. Cheng, M. Tang, Adsorption of methylene blue by phoenix tree leaf powder in a fixed-bed column: Experiments and prediction of breakthrough curves, Desalination 245 (2009) 284–297.
[16] W.S. Wan Ngah, L.C. Teong, R.H. Toh, M.A.M. Hanafiah, Utilization of chitosan-zeolite composite in the removal of Cu(II) from aqueous solution: Adsorption, desorption and fixed bed column studies, Chem. Eng. J. 209 (2012) 46–53.
[17] C.Y. Yin, M.K. Aroua, W.M.A.W. Daud, Fixed-bed adsorption of metal ions from aqueous solution on polyethyleneimine-impregnated palm shell activated carbon, Chem. Eng. J. 148 (2009) 8–14.
[18] R. Han, L. Zou, X. Zhao, Y. Xu, F. Xu, Y. Li, Y. Wang, Characterization and properties of iron oxide-coated zeolite as adsorbent for removal of copper(II) from solution in fixed bed column, Chem. Eng. J. 149 (2009) 123–131.
[19] Z. Xu, J. Cai, B. Pan, Mathematically modeling fixed-bed adsorption in aqueous systems, J. Zhejiang Univ.-Sci. A, 14 (2013) 155–176.
[20] M. Rožic, D. Ivanec Šipušic, L. Sekovanic, S. Miljanic, L. Curkovic, J. Hrenovic, Sorption phenomena of modification of clinoptilolite tuffs by surfactant cations, J. Colloid Interf. Sci., 331 (2009) 295–301.
[21] M. Rožić, S. Miljanić, Sorption of HDTMA cations on croatian natural mordenite tuff, J. Hazard. Mater. 185 (2011) 423–429.
[22] J. Xie, W. Meng, D. Wu, Z. Zhang, H. Kong, Removal of organic pollutants by surfactant modified zeolite: Comparison between ionizable phenolic compounds and non-ionizable organic compounds, J. Hazard. Mater. 231–232 (2012) 57–63.
[23] J. Zhang, J. Yu, W. An, J. Liu, Y. Wang, Y. Chen, J. Tai, M. Yang, Characterization of disinfection byproduct formation potential in 13 source waters in China, J. Environ. Sci. 23 (2011) 183–188.
[24] Y. Zhan, Z. Zhu, J. Lin, Y. Qiu, J. Zhao, Removal of humic acid from aqueous solution by cetylpyridinium bromide modified zeolite, J. Environ. Sci. 22 (2010) 1327–1334.
[25] P. Castaldi, L. Santona, S. Enzo, P. Melis, Sorption processes and XRD analysis of a natural zeolite exchanged with Pb^{2+}, Cd^{2+} and Zn^{2+} cations, J. Hazard. Mater. 156 (2008) 428–434.

[26] J. Lin, Y. Zhan, Adsorption of humic acid from aqueous solution onto unmodified and surfactant-modified chitosan/zeolite composites, Chem. Eng. J. 200–202 (2012) 202–213.
[27] K. Elaiopoulos, T. Perraki, E. Grigoropoulou, Monitoring the effect of hydrothermal treatments on the structure of a natural zeolite through a combined XRD, FTIR, XRF, SEM and N2-porosimetry analysis, Micropor. Mesopor. Mat. 134 (2010) 29–43.
[28] M. Rozwadowski, R. Wojsz, K.E. Wisniewski, J. Kornatowski, Description of adsorption equilibrium on type A zeolites with use of the Polanyi-Dubinin potential theory, Zeolites 9 (1989) 503–508.
[29] L. Abu-Lail, J.A. Bergendahl, R.W. Thompson, Adsorption of methyl tertiary butyl ether on granular zeolites: Batch and column studies, J. Hazard. Mater. 178 (2010) 363–369.
[30] L.B. McCusker, C. Baerlocher, Zeolite Structures, Elsevier, The Netherlands, 2001, pp. 37–67.
[31] M. Kruk, M. Jaroniec, Gas adsorption characterization of ordered organic−inorganic nanocomposite materials, Chem. Mater. 13 (2001) 3169–3183.
[32] K.J. Kim, H.G. Ahn, The effect of pore structure of zeolite on the adsorption of VOCs and their desorption properties by microwave heating, Micropor. Mesopor .Mat. 152 (2012) 78–83.
[33] P. Chutia, S. Kato, T. Kojima, S. Satokawa, Adsorption of As(V) on surfactant-modified natural zeolites, J. Hazard. Mater. 162 (2009) 204–211.
[34] P. Hudec, A. Smiešková, V. Jorík, Sensitivity of the C-constant of BET-Isotherm to the content of micropore volume in mesoporous matrix, Stud. Surf. Sci. Catal., Elsevier, 2008.
[35] R. Leyva-Ramos, A. Jacobo-Azuara, P.E. Diaz-Flores, R.M. Guerrero-Coronado, J. Mendoza-Barron, M.S. Berber-Mendoza, Adsorption of chromium(VI) from an aqueous solution on a surfactant-modified zeolite, Colliod Surface. A 330 (2008) 35–41.
[36] D.P. Serrano, J. Aguado, G. Morales, J.M. Rodríguez, A. Peral, M. Thommes, J.D. Epping, B.F. Chmelka, Molecular and meso- and macroscopic properties of hierarchical nanocrystalline ZSM-5 zeolite prepared by seed silanization, Chem. Mater. 21 (2009) 641–654.
[37] M. Jaroniec, J. Choma, M. Kruk, On the Applicability of the Horwath-Kawazoe method for pore size analysis of MCM-41 and related mesoporous materials, Elsevier, Stud. Surf. Sci. Catal. 128 (2000) 225–234.
[38] A. Gil, P. Grange, Application of the Dubinin–Radushkevich and Dubinin–Astakhov equations in the characterization of microporous solids, Colloids Surf., A 113 (1996) 39–50.
[39] A. Gil, S.A. Korili, G.Y. Cherkashinin, Extension of the Dubinin–Astakhov equation for evaluating the micropore size distribution of a modified carbon molecular sieve, J. Colloid Interface 262 (2003) 603–607.
[40] C. Nguyen, D.D. Do, The Dubinin–Radushkevich equation and the underlying microscopic adsorption description, Carbon 39 (2001) 1327–1336.
[41] Y. Yu, J.G. Shapter, R. Popelka-Filcoff, J.W. Bennett, A.V. Ellis, Copper removal using bio-inspired polydopamine coated natural zeolites, J. Hazard. Mater., 2014.
[42] K. Shams, S.J. Mirmohammadi, Preparation of 5A zeolite monolith granular extrudates using kaolin: Investigation of the effect of binder on sieving/adsorption properties using a mixture of linear and branched paraffin hydrocarbons, Micropor. Mesopor. Mat. 106 (2007) 268–277.
[43] K. Shams, H. Ahi, Synthesis of 5A zeolite nanocrystals using kaolin via nanoemulsion-ultrasonic technique and study of its sorption using a known kerosene cut, Micropor. Mesopor. Mat. 180 (2013) 61–70.
[44] Y. Iwai, N. Oka, T. Yamanishi, Influence of framework silica-to-alumina ratio on the water adsorption and desorption characteristics of MHI-CaX/CaY zeolite, J. Phys. Chem. Solids 70 (2009) 881–888.
[45] P.K. Bajpai, Synthesis of mordenite type zeolite, Zeolites 6 (1986) 2–8.
[46] K. Margeta, N.Z. Logar, M. Šiljeg, A. Farkas, Natural Zeolites in Water Treatment—How Effective is Their Use, Water Treatment, Zagreb, 2013 (Chapter 5).
[47] A.M. Yusof, N.A.N.N. Malek, Removal of Cr(VI) and As(V) from aqueous solutions by HDTMA-modified zeolite Y, J. Hazard. Mater. 162 (2009) 1019–1024.
[48] M. Rožić, Š. Cerjan-Stefanović, S. Kurajica, M.R. Maěefat, K. Margeta, A. Farkaš, Decationization and dealumination of clinoptilolite tuff and ammonium exchange on acid-modified tuff, J. Colloid Interf. Sci. 284 (2005) 48–56.
[49] A.F.P. Ferreira, M.C. Mittelmeijer-Hazeleger, A. Bliek, J.A. Moulijn, Influence of Si/Al ratio on hexane isomers adsorption equilibria, Micropor. Mesopor. Mat. 111 (2008) 171–177.
[50] G.D. Knowlton, T.R. White, Thermal study of types of water associated with clinoptilolite, Clays Clay Miner. 29 (1981) 403–411.
[51] Arletti, A. Martucci, A. Alberti, L. Pasti, M. Nassi, R. Bagatin, Location of MTBE and toluene in the channel system of the zeolite mordenite: Adsorption and host–guest interactions, J. Solid State Chem. 194 (2012) 135–142.
[52] A. Martucci, L. Pasti, M. Nassi, A. Alberti, R. Arletti, R. Bagatin, R. Vignola, R. Sticca, Adsorption mechanism of 1,2-dichloroethane into an organophilic zeolite mordenite: A combined diffractometric and gas chromatographic study, Microporous Mesoporous Mater. 151 (2012) 358–367.
[53] M. Canli, Y. Abali, S.U. Bayca, Removal of methylene blue natural and Ca and K-exchanged zeolite treated with hydrogen peroxide, Physicochem. Probl. Miner. Process 49 (2013) (2013) 481–496.
[54] Y. Park, G.A. Ayoko, R.L. Frost, Application of organoclays for the adsorption of recalcitrant organic molecules from aqueous media, J. Colloid Interface Sci. 354 (2011) 292–305.
[55] B. Sarkar, M. Megharaj, Y. Xi, G.S.R. Krishnamurti, R. Naidu, Sorption of quaternary ammonium compounds in soils: Implications to the soil microbial activities, J. Hazard. Mater. 184 (2010) 448–456.
[56] J. Schick, P. Caullet, J.-L. Paillaud, J. Patarin, C. Mangold-Callarec, Batch-wise nitrate removal from water on a surfactant-modified zeolite, Microporous Mesoporous Mater. 132 (2010) 395–400.
[57] R.M. Mohamed, A.A. Ismail, G. Kini, I. A. Ibrahim ,B. Koopman, Synthesis of highly ordered cubic zeolite A and its ion-exchange behavior, Colloids Surf., A 348 (2009) 87–92.
[58] A. Dominguez, A. Fernandez, N. Gonzalez, E. Iglesias, L. Montenegro, Determination of critical micelle

concentration of some surfactants by three techniques, J. Chem. Educ. 74 (1997) 1227–1231.
[59] S. Wang, W. Gong, X. Liu, B. Gao, Q. Yue, Removal of fulvic acids using the surfactant modified zeolite in a fixed-bed reactor, Sep. Purif. Technol. 51 (2006) 367–373.
[60] Z. Li, T. Burt, R.S. Bowman, Sorption of ionizable organic solutes by surfactant-modified zeolite, Environ. Sci. Technol. 34 (2000) 3756–3760.
[61] A.M. El-Kamash, Evaluation of zeolite A for the sorptive removal of Cs^{+} and Sr^{2+} ions from aqueous solutions using batch and fixed bed column operations, J. Hazard. Mater. 151 (2008) 432–445.
[62] S. M. Maliyekkal, A. K. Sharma, L. Philip, Manganese-oxide-coated alumina: A promising sorbent for defluoridation of water, Water Res. 40 (2006), 3497–3506.
[63] M.A. Stylianou, V.J. Inglezakis, K.G. Moustakas, S. P. Malamis, M. D. Loizidou, Removal of Cu(II) in fixed bed and batch reactors using natural zeolite and exfoliated vermiculite as adsorbents, Desalination 215 (2007) 133–142.
[64] T. Moriguchi, K. Yano, M. Tahara, K. Yaguchi, Metal-modified silica adsorbents for removal of humic substances in water, J. Colloid Interface Sci. 283 (2005) 300–310.
[65] X. Peng, Z. Luan, F. Chen, B. Tian, Z. Jia, Adsorption of humic acid onto pillared bentonite, Desalination 174 (2005) 135–143.
[66] M.N. Moura, M.J. Martín, F.J. Burguillo, A comparative study of the adsorption of humic acid, fulvic acid and phenol onto *Bacillus subtilis* and activated sludge, J. Hazard. Mater. 149 (2007) 42–48.
[67] A. Imyim, E. Prapalimrungsi, Humic acids removal from water by aminopropyl functionalized rice husk ash, J. Hazard. Mater. 184 (2010) 775–781.